Pictorial Essay | Gastrointestinal Imaging

https://doi.org/10.3348/kjr.2017.18.2.323
pISSN 1229-6929 · eISSN 2005-8330
Korean J Radiol 2017;18(2):323-335

Korean Journal of Radiology
KJR

Imaging Patterns of Intratumoral Calcification in the Abdominopelvic Cavity

Mi Hye Yu, MD, PhD, Young Jun Kim, MD, PhD, Hee Sun Park, MD, PhD, Sung Il Jung, MD, PhD, Hae Jeong Jeon, MD, PhD

All authors: Department of Radiology, Konkuk University Medical Center, Seoul 05030, Korea

Intratumoral calcification is one of the most noticeable of radiologic findings. It facilitates detection and provides information important for correctly diagnosing tumors. In the abdominopelvic cavity, a wide variety of tumors have calcifications with various imaging features, though the majority of such calcifications are dystrophic in nature. In this article, we classify the imaging patterns of intratumoral calcification according to number, location, and morphology. Then, we describe commonly-encountered abdominopelvic tumors containing typical calcification patterns, focusing on their differentiable characteristics using the imaging patterns of intratumoral calcification.

Keywords: *Abdominopelvic neoplasm; Calcification*

INTRODUCTION

Calcification is occasionally observed in tumors, regardless of the organ or type of tumor. It is a notable radiologic feature and one that potentially has clinical significance, since the identification of intratumoral calcification facilitates detection of the tumor as well as its differential diagnosis (1, 2). In the abdominopelvic cavity, various kinds of tumors such as, for instance, mucin-producing tumors, metastases, gastrointestinal tumors, solid pseudopapillary neoplasms (SPNs), and so on are frequently accompanied by intratumoral calcification (2-5). Furthermore, the imaging features of intratumoral calcification also differ according to the type of tumor. However, to date, prior case reports and series regarding intratumoral calcification have each focused on a specific single case or one particular tumor, and no study has addressed this issue comprehensively.

Therefore, in this article, we classify the imaging patterns of intratumoral calcification according to number, location, and morphology of the calcification. In addition, we briefly review the abdominopelvic tumors that frequently exhibit typical patterns of intratumoral calcification. We also describe the imaging features with a focus on the differentiable characteristics of the tumors using the pattern of calcification, together with representative cases.

Received July 19, 2016; accepted after revision October 20, 2016.
This work was supported by the Konkuk University Medical Center Research Grant 2014.
This work was lectured at the 37th Scientific Assembly and Annual Meeting of the Korean Society of Abdominal Radiology and presented as an educational exhibit at the 2015 RSNA Annual Meeting.

Corresponding author: Young Jun Kim, MD, PhD, Department of Radiology, Konkuk University Medical Center, 120-1 Neungdong-ro, Gwangjin-gu, Seoul 05030, Korea.
• Tel: (822) 2030-5494 • Fax: (822) 2030-5549
• E-mail: yjkim@kuh.ac.kr

Intratumoral Calcification and Imaging Modalities

Intratumoral calcification is a type of pathologic calcification. Pathologic calcification is defined as an abnormal calcium deposition in soft tissues. It occurs via

two mechanisms: metastatic and dystrophic. Metastatic calcification may be a result of systemic mineral imbalance, such as uremia or hyperparathyroidism; while dystrophic calcification may be a result of tissue injury, aging, disease, or malignancy (6, 7). Thus, intratumoral calcification is usually considered to be dystrophic calcification caused by degenerative changes of the tissue, such as necrosis or hemorrhage, with the exception of a few bone-forming tumors.

Calcification, as it appears on radiographs and CT images, is easily visible as a hyper-dense or radiopaque lesion, because calcification attenuates X-rays (8). In clinical practice, CT is regarded as the gold standard for the identification of calcified lesions (9, 10).

On US, calcification exhibits a hyperechoic appearance, as it contains high-intensity reflectors. Depending on the size and characteristics of the surface structure of calcification, posterior acoustic shadowing may or may not be evident (8). Occasionally, a color Doppler twinkling artifact (color comet tail artifact) is observed because this artifact is generated by a strongly reflecting medium with a rough interface and because most of the calcifications are small and have a rough surface (11, 12). Therefore, the color Doppler twinkling artifact is a helpful sign for identifying small calcifications and thus can improve diagnostic confidence (12).

On MR, calcification shows various nonspecific signal intensities on conventional spin echo T1- or T2-weighted images (9, 13). Therefore, it difficult to definitively identify the intensities as calcium deposits, and thus small calcifications are easily missed on MR. However, dense calcification typically appears as a signal-void area because it has a very lower water content (8). In a gradient-echo sequence, calcification usually appears as being hypointense and cannot be differentiated from hemorrhage (9).

Imaging Patterns of Intratumoral Calcification

To date, a multitude of descriptive expressions have been used unsystematically to describe imaging patterns of calcification: fine, popcorn, granular, punctate, speculated, eggshell, miliary, and so on. We classify several patterns of intratumoral calcification according to the number, location, and morphology of the calcification (Fig. 1). In general, calcification in tumors can be single (solitary) or multiple, and can be located in the peripheral or the central portion of the tumor or at the internal septa. According to its morphology, intratumoral calcification is classified as having patterns which may be punctate (round), amorphous (irregularly shaped), curvilinear (curved line), or rim (eggshell, cyst-wall like appearance).

Then, based on the imaging pattern of intratumoral calcification, we categorize commonly-encountered abdominopelvic tumors which frequently show a typical calcification pattern as follows: mucinous adenocarcinoma, mucinous cystic neoplasm, metastasis, hemangioma, mature cystic teratoma, and miscellaneous tumors.

Mucinous Adenocarcinoma

Mucinous adenocarcinoma is a rare subtype (10–15%) of adenocarcinoma that usually occurs in the stomach and the colorectum. It is histologically defined as an extracellular mucin pool of > 50% of the tumor volume (2, 14). Mucinous adenocarcinoma of the stomach shows typical CT findings with a thickening of the diffusely low-attenuating middle or outer layer (corresponding to the mucin pool) and a presence of associated multiple, punctate calcifications (9.5%) (Figs. 2, 3) (15). The presence of mucin is thought to act as an ion-exchange resin, and mucin may be an important factor both for calcium deposition within gastrointestinal carcinoma and in its metastasis (3, 16, 17). Compared with non-mucinous carcinoma, mucinous adenocarcinoma in the colorectum shows more eccentric bowel wall thickening, heterogeneous enhancement, a greater area of low attenuation, and more frequent intratumoral calcification (21%) (2).

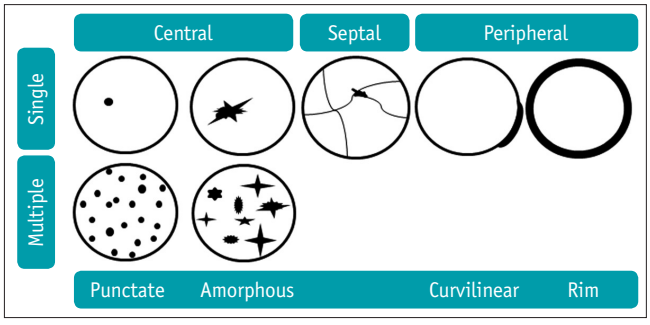

Fig. 1. Imaging patterns of intratumoral calcification according to number, location, and morphology. Calcification is seen–in tumors–in single or multiple form, and can be located in center or peripheral portion of tumor, or at internal septa (septal). Punctate (round), amorphous (irregularly shaped), curvilinear (curved line), or rim (eggshell, cyst-wall like appearance) calcification is in evidence.

Korean Journal of Radiology
KJR

Mucinous Cystic Neoplasm

Mucinous cystic neoplasm is currently defined as a cyst-forming epithelial neoplasm composed of mucin-producing epithelium and associated with ovarian-type subepithelial stroma (18, 19).

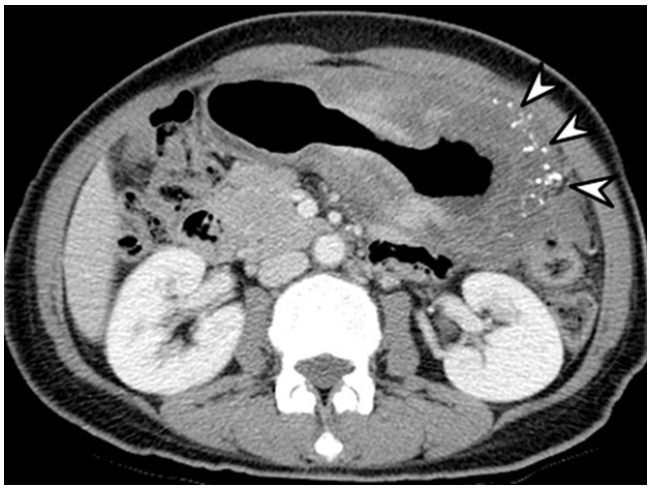

Fig. 2. Mucinous adenocarcinoma of stomach in 60-year-old female. Axial contrast-enhanced CT image shows diffuse, low-attenuated wall thickening containing multiple punctate calcifications (arrowheads) involving high-to-low body of stomach. These CT findings are characteristic imaging features of gastric mucinous adenocarcinoma.

Fig. 3. Mucinous adenocarcinoma of colon in 22-year-old female. Coronal contrast-enhanced CT image reveals segmental, low-attenuated wall thickening (arrow) at descending colon, causing upstream colonic obstruction (asterisk). Several punctate calcifications (arrowheads) are seen in low-attenuated, thickened colon wall. Patient underwent left hemicolectomy and was diagnosed with mucinous adenocarcinoma.

Pancreas

Mucinous cystic neoplasm of the pancreas is a relatively uncommon tumor with a predominance among females (> 95%) and a predilection for the pancreas body or tail (20). If mucinous cystic neoplasm is suspected from imaging, complete surgical excision is advocated–as the tumor has malignant potential. Mucinous cystic neoplasm from the pancreas shares common clinical and pathologic characteristics with mucinous cystic neoplasm that arises in the liver and ovary (21). On cross-sectional imaging, mucinous cystic neoplasm of the pancreas appears as a well-capsulated, unilocular, macrocystic lesion with or without septation or mural nodule (21-23). Calcification is found in 10–25% of cases with a peripheral, curvilinear pattern or septal location (Figs. 4, 5) (1, 23). Intratumoral calcification occasionally enables differentiation of mucinous cystic neoplasms from serous cystic neoplasms, which frequently have central calcification within the central fibrous scar (1).

Liver

Mucinous cystic neoplasm of the liver is a rare neoplasm of the biliary system and has been previously referred to as biliary cystadenoma and biliary cystadenocarcinoma (18). It occurs usually in the intrahepatic bile duct (85%), and occurs predominantly among middle-aged females (23). On cross-sectional imaging, mucinous cystic neoplasm of the liver appears as a solitary, well-encapsulated cystic

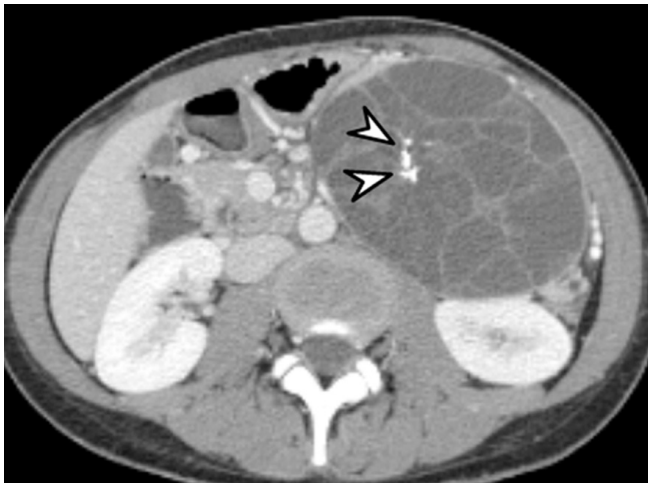

Fig. 4. Mucinous cystic neoplasm of pancreas in 31-year-old female. Axial contrast-enhanced CT image demonstrates large, well-defined, low-attenuated cystic mass with multiple internal septa in pancreatic tail (not shown). Typical septal calcifications (arrowheads) are noted within lesion. Distal pancreatectomy was performed, and mucinous cystic neoplasm was diagnosed.

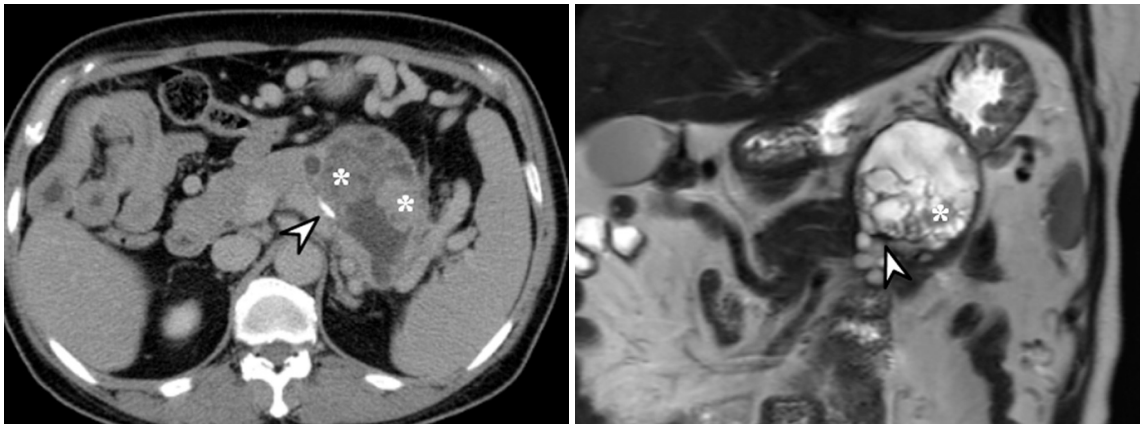

Fig. 5. Mucinous cystic neoplasm of pancreas in 51-year-old female.
A. Bulging, contoured, low-attenuated cystic mass in pancreatic tail is seen on axial contrast-enhanced CT image. There are multifocal enhancing solid components (asterisks) in mass, and peripheral curvilinear calcification (arrowhead) is also in evidence. **B.** This coronal T2-weighted MR image demonstrates presence of cystic mass with internal solid portion (asterisk). Peripheral curvilinear calcification (arrowhead) of lesion is seen as region of hyposignal intensity. After distal pancreatectomy, mucinous cystic neoplasm with associated invasive carcinoma was diagnosed.

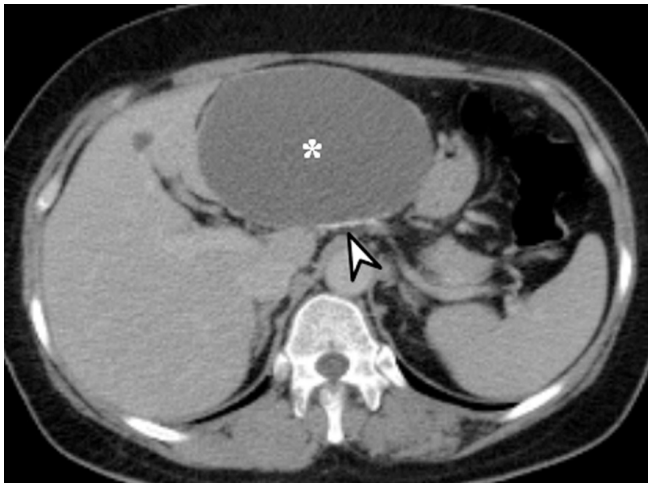

Fig. 6. Mucinous cystic neoplasm of liver in 56-year-old female. Large, well-defined, unilocular cystic mass (asterisk) is located in left lateral section of liver as shown on axial contrast-enhanced CT image. Peripheral curvilinear calcification (arrowhead) is noted, and there is no enhancing solid component. Hepatic segmentectomy was performed, and lesion was confirmed as being mucinous cystic neoplasm (biliary cystadenoma) with dystrophic calcification and containing internal hemorrhage.

mass with internal septa and/or mural nodules (23, 24). Intratumoral calcification is rarely found, but was reported in 47% (7/15) of the cases in a recent study (19). It is usually seen within the wall (peripheral) (Fig. 6) and the septa (septal) (Fig. 7) (24). However, calcification can be also seen in intraductal papillary neoplasms and solitary bile duct cysts, which should be differentiated from mucinous cystic neoplasms of the liver (19). Some radiologic features, including the presence of internal septa and solid mural nodules, are more likely to be mucinous cystic neoplasms with invasive carcinoma (biliary cystadenocarcinoma) (25).

Appendix

The descriptive term "mucocele" refers to luminal distension of the appendix by the mucin, regardless of the underlying pathology (26). It can be caused by a variety of non-neoplastic, benign neoplastic, and malignant conditions; however, mucinous neoplasm of the appendix is the most common cause of mucocele (23). The WHO classification recognizes 3 main categories of mucinous neoplasm of the appendix: mucinous adenoma, low-grade mucinous neoplasm, and mucinous adenocarcinoma (27, 28). CT is preferred as the modality of choice because it depicts well the anatomical relationship between the cystic mass and cecum, as well as the tissue characteristics. On CT, an appendiceal mucinous neoplasm appears as a round or tubular cystic mass with an enhancing wall in the expected position of the appendix (Fig. 8) (23). Curvilinear, peripheral (mural) calcification occurs in < 50% of cases (26, 29) (Figs. 8, 9), and it is highly suggestive of the diagnosis. Soft tissue mass, wall thickening, and irregularity raise the suspicion of malignancy (Fig. 9) (28, 30).

Metastasis

Intratumoral calcification is also seen in metastatic lesions. First, some metastases may develop calcifications because of the histology of the primary malignancy. Metastasis from mucinous adenocarcinoma most commonly contains calcification with a punctate pattern, similar to

Korean Journal of Radiology
KJR

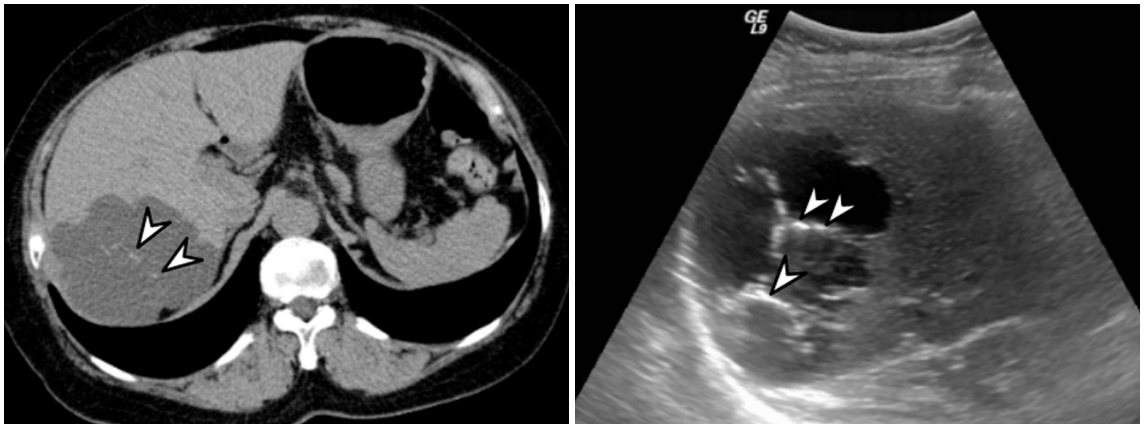

A B

Fig. 7. Mucinous cystic neoplasm of liver, in 75-year-old female.
A. On axial pre-contrast CT image, lobulating, contoured cystic mass is located in segment 7 of liver. Fine septal calcifications (arrowheads) are seen. **B.** On ultrasound scan, fine septal calcifications (arrowheads), within cystic mass, are seen as echogenic lesions with posterior acoustic shadowing. After hepatic tumorectomy, mucinous cystic neoplasm (biliary cystadenoma) was diagnosed.

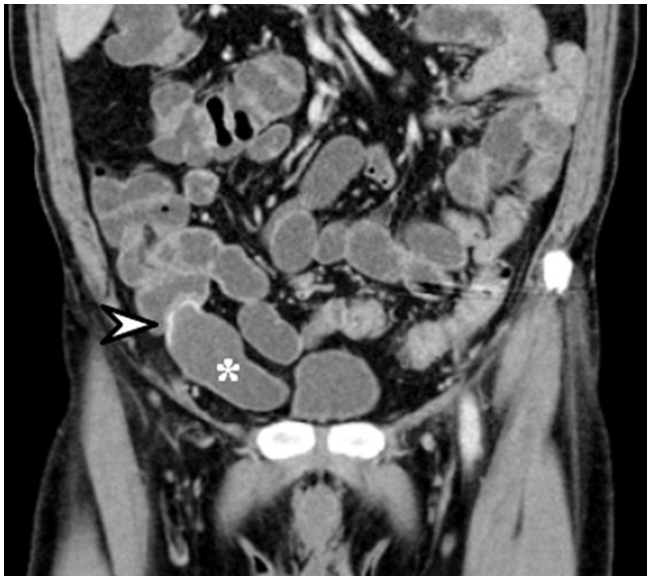

Fig. 8. Mucinous neoplasm of appendix in 61-year-old male.
Coronal contrast-enhanced CT image demonstrates cystic dilatation of appendix (asterisk) without evidence of acute inflammation. Curvilinear calcification (arrowhead) is seen at proximal appendiceal wall. Appendectomy was performed, and low-grade appendiceal mucinous neoplasm was diagnosed.

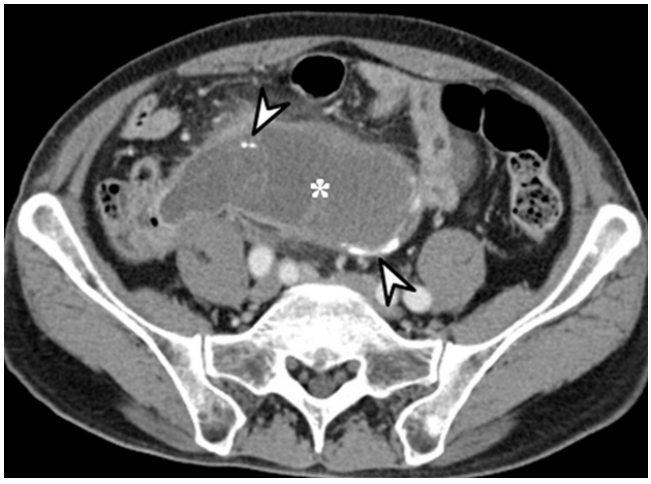

Fig. 9. Mucinous adenocarcinoma of appendix in 72-year-old male. Axial contrast-enhanced CT image reveals cystic dilatation of appendix (asterisk) with peripheral, curvilinear calcifications (arrowheads). Internal, mild enhancing solid portions and perilesional fatty infiltrations are demonstrated. After appendectomy, mucinous adenocarcinoma was diagnosed.

the primary lesion (3, 17). Metastasis from other primary malignancies such as papillary thyroid cancer, breast cancer, and chondrosarcoma are rare, but may show calcification (Fig. 10) (3).

Secondarily, after systemic chemotherapy or radiation therapy, dystrophic calcification can develop in the metastatic lesion. Calcification in colorectal liver metastasis after chemotherapy is occasionally encountered in clinical practice. Calcification in hepatic metastasis shows a variable pattern and distribution (central and peripheral), and may develop or change during therapy (Fig. 11) (31). Calcification in colorectal liver metastasis is generally considered to be a good indicator of the response to treatment (32).

Hemangioma

Hemangioma is a benign vascular tumor and is composed of a blood-filled space lined by single or multiple layers of endothelial cells and a thin fibrous stroma (3). In the abdominal pelvic cavity, hepatic hemangioma is the most common. It has the characteristic imaging features of

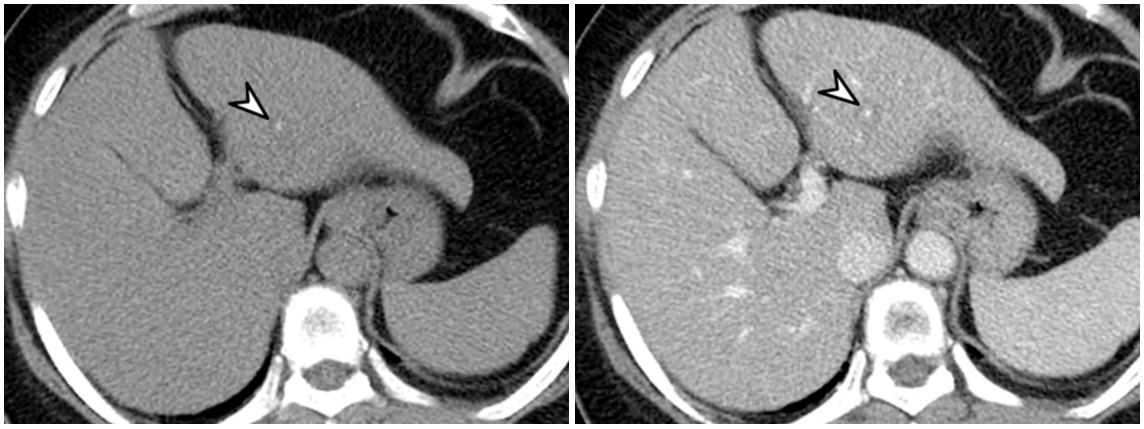

A B

Fig. 10. Hepatic metastasis from breast cancer in 60-year-old female.
A, B. Small low-attenuated lesion with tiny calcification (arrowheads) is noted in left lateral section of liver. Metastatic tumor from breast cancer was confirmed via percutaneous biopsy.

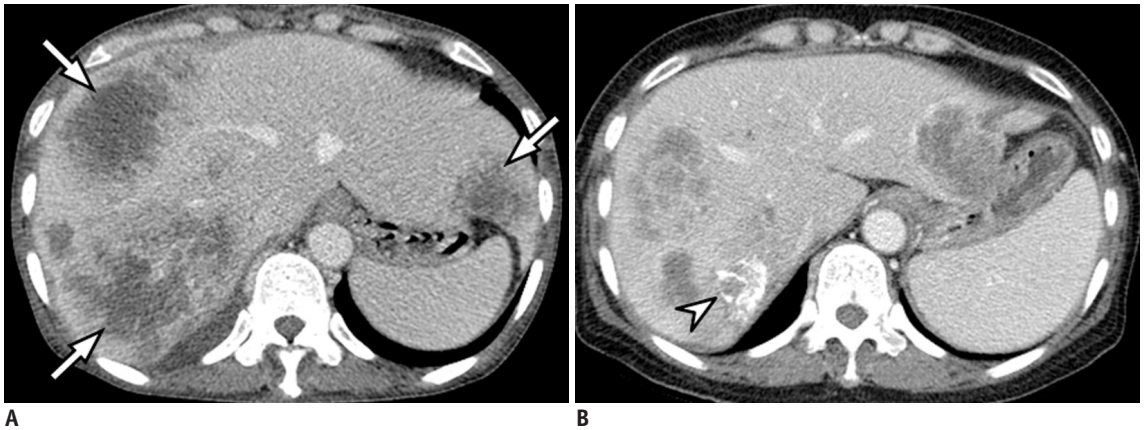

A B

Fig. 11. Hepatic metastases from colon cancer in 60-year-old female.
A. Multiple low-attenuated metastases (arrows) are located in both liver lobes on axial contrast-enhanced CT image. **B.** On follow-up CT image taken after patient underwent chemotherapy, multiple previous metastases are decreased in size, and amorphous intratumoral calcification (arrowhead) is newly developed.

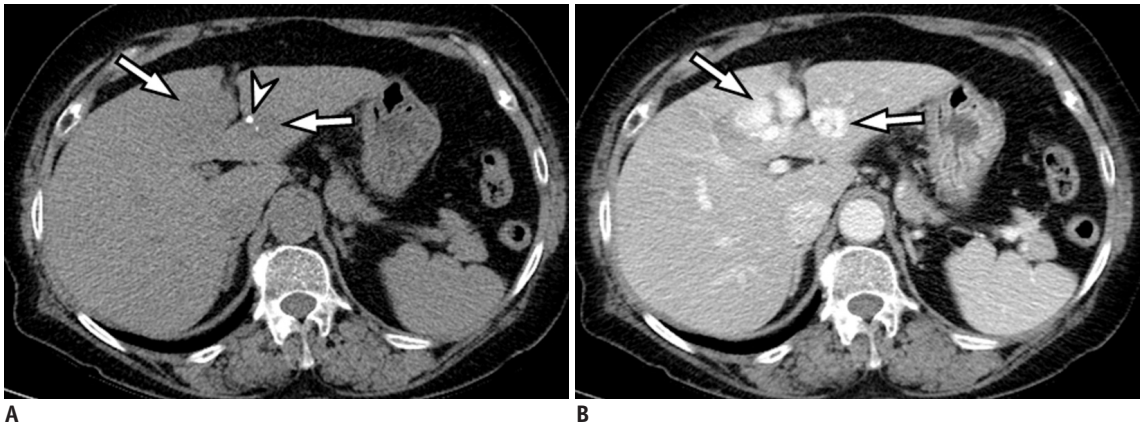

A B

Fig. 12. Hepatic hemangiomas in 67-year-old female.
A, B. There are two small hemangiomas (arrows) in left lobe of liver. On axial pre-contrast CT scan **(A)**, small punctate calcification (arrowhead), known as phlebolith, is seen at small hemangioma (arrows) in left lateral section. Although dynamic contrast-enhanced CT that showed typical progressive centripetal enhancement is not seen, hemangiomas (arrows) show peripheral nodular enhancement and punctate calcification on axial portal venous phase image **(B)**.

Korean Journal of Radiology
KJR

a progressive peripheral to central fill-in enhancement pattern on dynamic imaging (33). Calcification is rarely demonstrated in hepatic hemangioma but is often found in sclerosing hemangioma or giant hemangioma (34-36). Calcification in hemangioma is known as a phlebolith, which arises because of thrombosis from inflammation or stasis of blood flow (37). It usually appears as a discrete, rounded pattern (punctate) with a central or peripheral location (Figs. 12, 13) (33-35).

Hemangioma of the gastrointestinal tract is rare, and gastrointestinal bleeding is the most common clinical presentation. Hemangioma may occur anywhere in the gastrointestinal tract; the small bowel is the most frequent site, and the colon is the second most frequent site (38). Most hemangiomas are seen to be pedunculated intraluminal polypoid masses, but occasionally they have an infiltrative submucosal growth pattern (39). In the colon, rectosigmoid is the most commonly involved colonic segment; and colorectal hemangioma shows characteristic imaging features of transmural enhanced bowel wall thickening containing multiple, punctate calcifications (phleboliths) (Fig. 14) (38-40). The presence of multiple, punctate phleboliths is the pathognomonic imaging

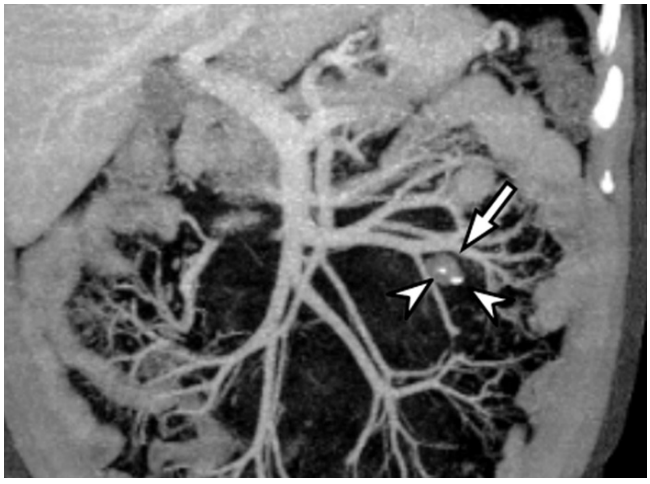

Fig. 13. Mesenteric hemangioma in 47-year-old male. On coronal, maximum-intensity projection CT image, small, round, soft tissue lesion is found in left-sided small bowel mesentery (arrow). Two small punctate calcifications (arrowheads) are seen within lesion. After mass excision, this lesion was confirmed as being mesenteric hemangioma.

Fig. 14. Sigmoid colon hemangioma in 22-year-old male. Axial contrast-enhanced CT image demonstrates segmental concentric bowel wall thickening (arrows) with multiple punctate calcifications (arrowheads, phleboliths) involving sigmoid colon. This multiple punctate calcification pattern is characteristic imaging feature of gastrointestinal hemangioma.

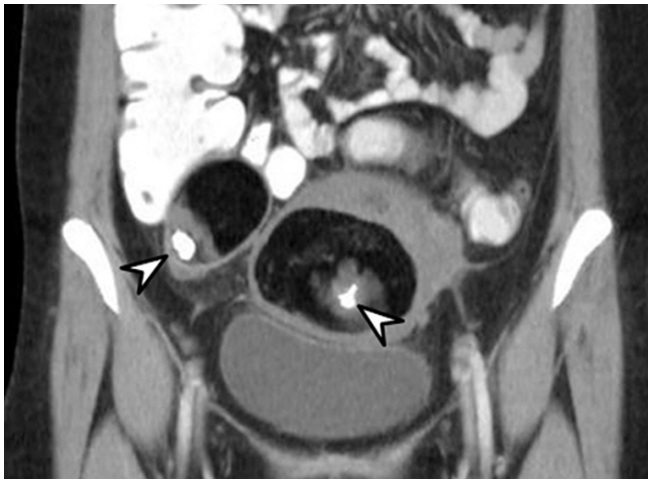

Fig. 15. Mature cystic teratomas in 40-year-old female. On coronal contrast-enhanced CT image, bilateral ovarian fatty masses containing punctate calcification (arrowheads) are visible. These are pathognomonic radiologic findings of mature cystic teratoma.

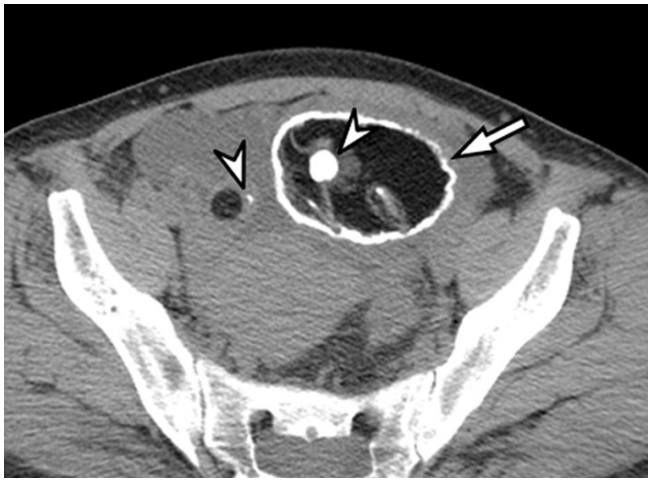

Fig. 16. Mature cystic teratomas in 55-year-old female. Bilateral mature cystic teratomas are found on axial pre-contrast CT image. In left mature cystic teratoma, presence of peripheral, thick, rim calcification (arrow) and central punctate calcification (arrowhead) are simultaneously noted. Right mature cystic teratoma contains single punctate calcification (arrowhead).

feature of gastrointestinal hemangioma that enables its differentiation from carcinoma (39).

Mature Cystic Teratoma

Mature cystic teratoma, also called dermoid cyst, is a cystic tumor of the ovary. The tumor is composed of well-differentiated tissues from at least two of the three germ cell layers (41). Most cases are asymptomatic; however they, can cause acute abdominal symptoms by torsion or rupture of the tumor (42). On CT, fat attenuation within a cyst with or without calcification is diagnostic of mature cystic teratoma (41, 43, 44). Teeth or other calcifications are frequently seen (56%) (44, 45). When bone or teeth are present, they tend to be located within the Rokitansky nodule (41, 46). Thus, intratumoral calcification in mature cystic teratoma usually appears as a single, punctate pattern within the mass (Fig. 15) (41, 47). Occasionally, it is possible to observe unusual dense rim calcification of the cyst wall (Fig. 16) (46-48).

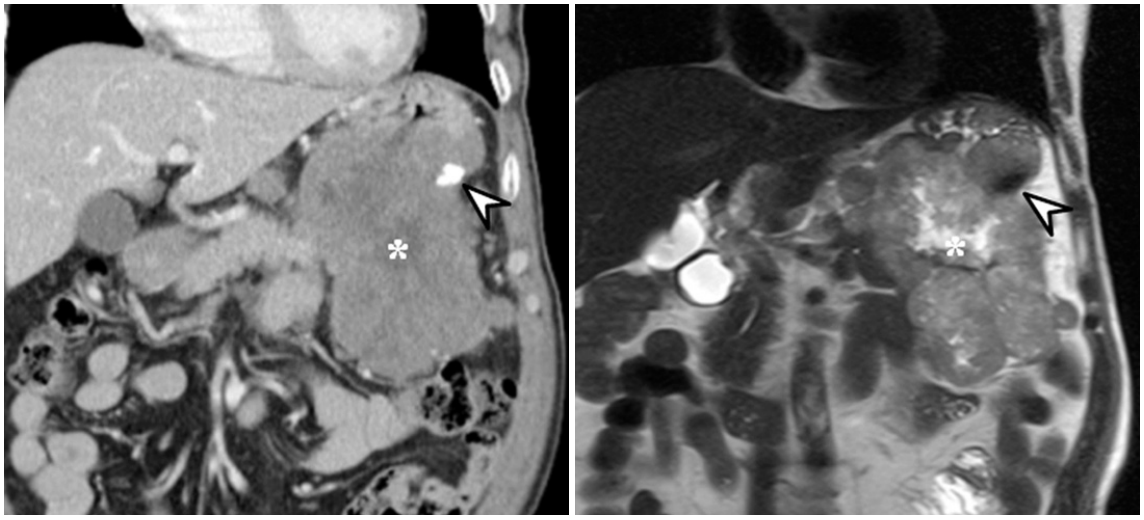

A B

Fig. 17. Gastrointestinal stromal tumor in 61-year-old male.
A. Exophytic lobulating contoured enhancing mass is seen in stomach high-body greater curvature on coronal contrast-enhanced CT image. Mass contains small, dense punctate calcification (arrowhead) and internal, low-density necrotic portion (asterisk). **B.** On coronal T2-weighted MR image, small dense punctate calcification (arrowhead) is seen as region of hyposignal intensity. Internal necrotic portion (asterisk) within mass appears as region of high signal intensity. Gastrointestinal stromal tumor was confirmed.

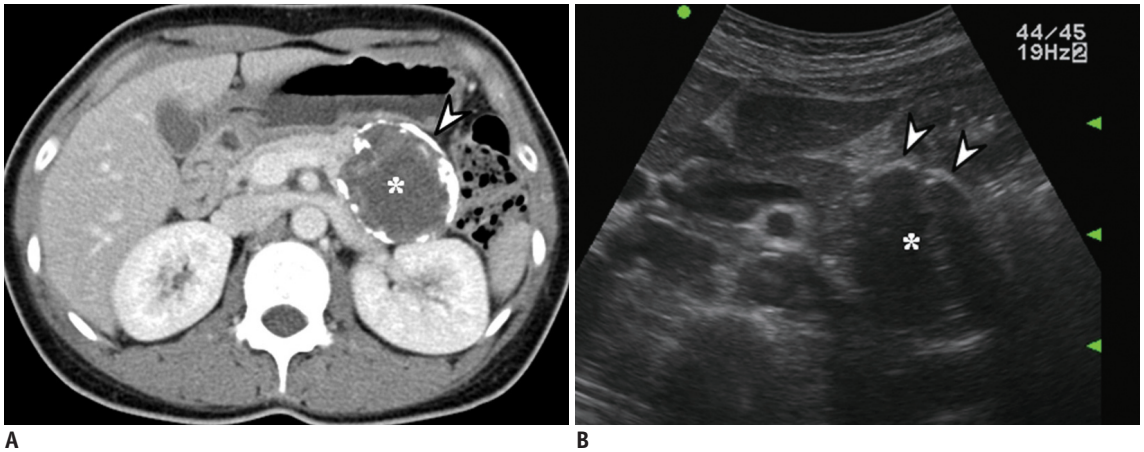

A B

Fig. 18. Solid pseudopapillary neoplasm of pancreas in 28 year-old female.
A. On axial contrast-enhanced CT image, low density mass (asterisk) with thick peripheral, rim calcification (arrowhead) is located in pancreatic tail. Main pancreatic duct is not dilated. **B.** On ultrasound scan, bulging contoured mass (asterisk) is suspected in pancreatic tail. Peripheral, rim calcification (arrowheads) of mass appears as hyperechogenicity with posterior acoustic presentation. Solid pseudopapillary neoplasm was diagnosed after distal pancreatectomy.

Korean Journal of Radiology
KJR

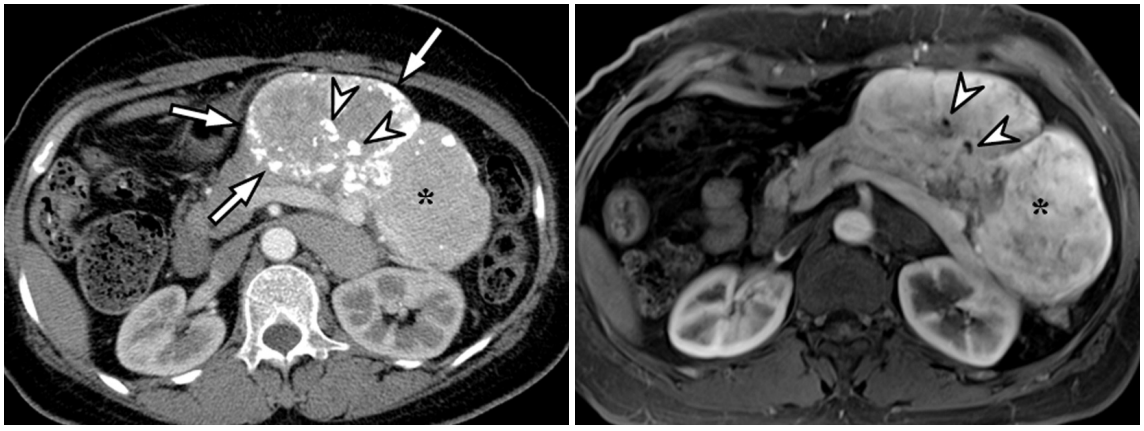

A B

Fig. 19. Pancreatic neuroendocrine tumor in 54-year-old female.
A. On axial contrast-enhanced CT image, large lobulating contoured hypervascular mass (asterisk) is located in pancreatic tail. Lesion contains multiple amorphous calcifications (arrows and arrowheads) at central and peripheral portions of mass. **B.** On contrast-enhanced T1-weighted image, dense calcifications (arrowheads) appear as dark signal intensity at center of mass (asterisk). However, other peripheral amorphous calcifications (arrows on **A**) are not clearly visualized. This mass was confirmed as neuroendocrine tumor (grade 2) after distal pancreatectomy.

Fig. 20. Multiple schwannomas in 39-year-old female. Coronal contrast-enhanced CT image demonstrates multiple round masses (asterisks) in retroperitoneum, which are confirmed as schwannomas. Punctate and curvilinear calcifications (arrowheads) are seen in some tumors.

Miscellaneous Tumors

Gastrointestinal Stromal Tumor (GIST)

Gastrointestinal stromal tumor (GIST) is the most common primary mesenchymal tumor of the gastrointestinal tract, and arises from the interstitial cell of Cajal (49). Generally, GIST is defined as a KIT (CD117)-positive tumor with a characteristic histologic feature (50). The radiologic appearance of GIST depends on the tumor size: a small GIST is seen as a well-defined mass with homogeneous enhancement, whereas a large GIST is seen as an exophytic heterogeneously enhancing mass with intratumoral hemorrhage or necrosis (49, 51). Calcification in a GIST is unusual (3–10%) and it may occur as a punctate pattern (Fig. 17) (51-53).

Solid Pseudopapillary Neoplasm (SPN)

Solid pseudopapillary neoplasms is a rare neoplasm of the pancreas that typically occurs in young females (54). The characteristic finding of SPN is a large, solitary, well-encapsulated mass with varying amounts of intratumoral hemorrhage or cystic component (55, 56). Intratumoral calcification is occasionally associated with SPN; and a peripheral curvilinear, rim (eggshell), or punctate pattern is usually seen (Fig. 18) (5).

Pancreatic Neuroendocrine Tumor (PNET)

Pancreatic neuroendocrine tumor (PNET) is a rare pancreatic neoplasm which demonstrates neuroendocrine differentiation (57). It is classified as functioning or non-

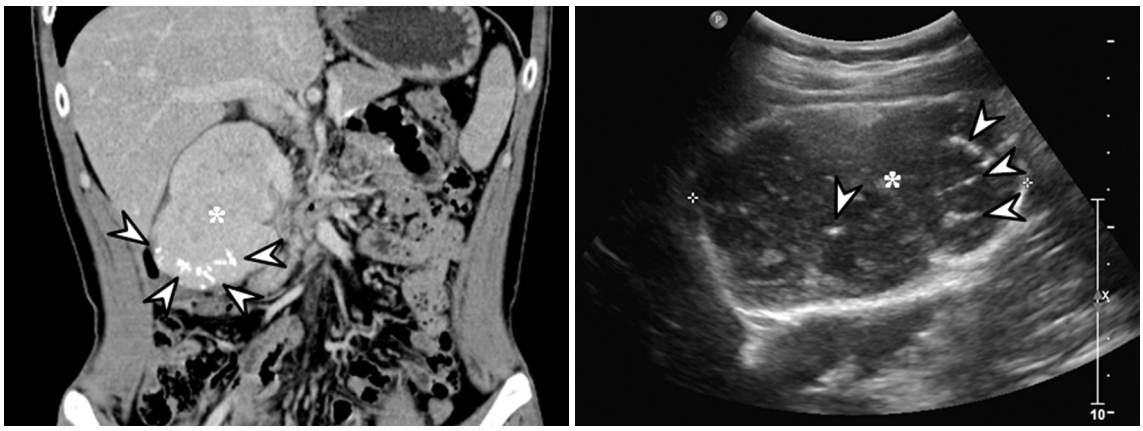

A B

Fig. 21. Castleman disease in 30-year-old male.
A. On coronal contrast-enhanced CT image, well-defined hypervascular retroperitoneal mass (asterisk) is found. Multiple amorphous calcifications (arrowheads) are noted within mass. **B.** On ultrasound scan, well-defined hypoechoic mass (asterisk) is revealed. Multiple intratumoral calcifications (arrowheads) are seen as echogenic portions with or without posterior acoustic shadowing. After mass excision, lesion was confirmed as Castleman disease.

functioning by hormonogenesis, and non-functional tumors currently account for the majority of newly diagnostic PNETs (up to 60–80%) (58). On imaging, a functioning PNET is typically found as a small (1–2 cm) hypervascular mass, whereas a non-functioning PNET appears as a relatively larger heterogeneous mass and commonly contains calcification, necrosis, or cystic change (59, 60). Calcification is found in approximately 20% (30/133) of them, and large tumors were more likely to be associated with calcification regardless of whether they are either functioning or non-functioning tumors (61). The pattern of calcification is very diverse and includes punctate, coarse (amorphous), and multiple pattern (Fig. 19) (60, 62). Calcification has often been thought to be indicative of a malignant lesion (58, 62). A recent study, however, found no significant correlation between the calcification and tumor grade (63). Intratumoral calcification can be helpful in differentiating PNET from pancreatic adenocarcinoma, because only 2% of adenocarcinomas show calcification as compared with 20% of PNETs (64).

Neurogenic Tumors

Neurogenic tumor is classified into ganglion cell origin (e.g., neuroblastoma, usually in children), paraganglionic system origin (e.g., pheochromocytoma, paraganglioma), and nerve sheath origin (e.g., neurilemmoma, so called schwannoma) (65). In the abdominal cavity, the tumor usually occurs in the retroperitoneum or the adrenal gland. It commonly appears as a well-circumscribed, smooth, or lobulating mass. Calcification may be seen in all types of neurogenic tumors with various patterns (Fig. 20) (65).

Castleman Disease

Castleman disease is an uncommon, benign lymphoproliferative disorder characterized by hyperplasia of the lymphoid follicles (66). Approximately 70% of cases are located in the thorax; 10–15% in the neck; and 10–15% in the abdomen, retroperitoneum, and pelvis (67, 68). Castleman disease commonly presents as single, well-circumscribed enhancing mass of varying locations in the abdomen and pelvis. Intratumoral calcification is reported in up to 31% (5/16) of cases of Castleman disease of the abdomen and pelvis (69). A variety of calcification patterns including punctate, peripheral, central, and arborizing patterns can be seen (Fig. 21) (66, 69). The presence of calcification may help in differentiating Castleman disease from lymphoma, since calcification would be rare in untreated lymphoma (70).

CONCLUSION

Intratumoral calcification exhibits various imaging patterns in various types of abdominopelvic tumors. However, several commonly-encountered tumors have a tendency towards showing typical patterns of intratumoral calcification. Although a specific diagnosis of a precise kind of tumor may not always be possible using only intratumoral calcification, imaging patterns of intratumoral calcification can help to facilitate accurate diagnosis and improve diagnostic confidence with regards to abdominopelvic

Korean Journal of Radiology
KJR

tumors. Therefore, it is useful to be aware of, and to be familiar with, the imaging patterns of intratumoral calcification in abdominopelvic tumors.

REFERENCES

1. Curry CA, Eng J, Horton KM, Urban B, Siegelman S, Kuszyk BS, et al. CT of primary cystic pancreatic neoplasms: can CT be used for patient triage and treatment? *AJR Am J Roentgenol* 2000;175:99-103
2. Ko EY, Ha HK, Kim AY, Yoon KH, Yoo CS, Kim HC, et al. CT differentiation of mucinous and nonmucinous colorectal carcinoma. *AJR Am J Roentgenol* 2007;188:785-791
3. Paley MR, Ros PR. Hepatic calcification. *Radiol Clin North Am* 1998;36:391-398
4. Izawa N, Sawada T, Abiko R, Kumon D, Hirakawa M, Kobayashi M, et al. Gastrointestinal stromal tumor presenting with prominent calcification. *World J Gastroenterol* 2012;18:5645-5648
5. Baek JH, Lee JM, Kim SH, Kim SJ, Kim SH, Lee JY, et al. Small (<or=3 cm) solid pseudopapillary tumors of the pancreas at multiphasic multidetector CT. *Radiology* 2010;257:97-106
6. Giachelli CM. Ectopic calcification: gathering hard facts about soft tissue mineralization. *Am J Pathol* 1999;154:671-675
7. Agarwal A, Yeh BM, Breiman RS, Qayyum A, Coakley FV. Peritoneal calcification: causes and distinguishing features on CT. *AJR Am J Roentgenol* 2004;182:441-445
8. Leyendecker JR, Tchelepi H. *Lesion composition*. In: Dalrymple NC, Leyendecker JR, Oliphant M, eds. *Problem solving in abdominal imaging*, 1st ed. Philadephia: Elsevier, 2009:e1-e20
9. Wu Z, Mittal S, Kish K, Yu Y, Hu J, Haacke EM. Identification of calcification with MRI using susceptibility-weighted imaging: a case study. *J Magn Reson Imaging* 2009;29:177-182
10. Roy B, Verma S, Awasthi R, Rathore RK, Venkatesan R, Yoganathan SA, et al. Correlation of phase values with CT Hounsfield and R2* values in calcified neurocysticercosis. *J Magn Reson Imaging* 2011;34:1060-1064
11. Rahmouni A, Bargoin R, Herment A, Bargoin N, Vasile N. Color Doppler twinkling artifact in hyperechoic regions. *Radiology* 1996;199:269-271
12. Kim HC, Yang DM, Jin W, Ryu JK, Shin HC. Color Doppler twinkling artifacts in various conditions during abdominal and pelvic sonography. *J Ultrasound Med* 2010;29:621-632
13. Sarmiento de la Iglesia MM, Lecumberri Cortés G, Lecumberri Cortés I, Oleaga Zufiria L, Isusi Fontan M, Grande Icaran D. [Intracranial calcifications on MRI]. *Radiologia* 2006;48:19-26
14. Hu B, El Hajj N, Sittler S, Lammert N, Barnes R, Meloni-Ehrig A. Gastric cancer: classification, histology and application of molecular pathology. *J Gastrointest Oncol* 2012;3:251-261
15. Park MS, Yu JS, Kim MJ, Yoon SW, Kim SH, Noh TW, et al. Mucinous versus nonmucinous gastric carcinoma: differentiation with helical CT. *Radiology* 2002;223:540-546
16. Ghahremani GG, Meyers MA, Port RB. Calcified primary tumors of the gastrointestinal tract. *Gastrointest Radiol* 1978;2:331-339
17. Stoupis C, Taylor HM, Paley MR, Buetow PC, Marre S, Baer HU, et al. The Rocky liver: radiologic-pathologic correlation of calcified hepatic masses. *Radiographics* 1998;18:675-685; quiz 726
18. Bosman FT, Cameron JL, Hruban RH, Theise ND. *WHO classification of tumours of the digestive system*, 4th ed. Lyon: IARC Press, 2010:217-224, 236-238, 254-261
19. Kim HJ, Yu ES, Byun JH, Hong SM, Kim KW, Lee JS, et al. CT differentiation of mucin-producing cystic neoplasms of the liver from solitary bile duct cysts. *AJR Am J Roentgenol* 2014;202:83-91
20. Farrell JJ. Prevalence, diagnosis and management of pancreatic cystic neoplasms: current status and future directions. *Gut Liver* 2015;9:571-589
21. Buetow PC, Rao P, Thompson LD. From the Archives of the AFIP. Mucinous cystic neoplasms of the pancreas: radiologic-pathologic correlation. *Radiographics* 1998;18:433-449
22. Sahani DV, Kadavigere R, Saokar A, Fernandez-del Castillo C, Brugge WR, Hahn PF. Cystic pancreatic lesions: a simple imaging-based classification system for guiding management. *Radiographics* 2005;25:1471-1484
23. Lee NK, Kim S, Kim HS, Jeon TY, Kim GH, Kim DU, et al. Spectrum of mucin-producing neoplastic conditions of the abdomen and pelvis: cross-sectional imaging evaluation. *World J Gastroenterol* 2011;17:4757-4771
24. Qian LJ, Zhu J, Zhuang ZG, Xia Q, Liu Q, Xu JR. Spectrum of multilocular cystic hepatic lesions: CT and MR imaging findings with pathologic correlation. *Radiographics* 2013;33:1419-1433
25. Buetow PC, Buck JL, Pantongrag-Brown L, Ros PR, Devaney K, Goodman ZD, et al. Biliary cystadenoma and cystadenocarcinoma: clinical-imaging-pathologic correlations with emphasis on the importance of ovarian stroma. *Radiology* 1995;196:805-810
26. Pickhardt PJ, Levy AD, Rohrmann CA Jr, Kende AI. Primary neoplasms of the appendix: radiologic spectrum of disease with pathologic correlation. *Radiographics* 2003;23:645-662
27. Carr N, Sobin L. *Tumors of the appendix*. In: Bosman FT, Carneiro F, Hruban RH, Theise ND, eds. *WHO classification of tumours of the digestive system*, 4th ed. Lyon: IARC Press, 2010:122-125
28. Tirumani SH, Fraser-Hill M, Auer R, Shabana W, Walsh C, Lee F, et al. Mucinous neoplasms of the appendix: a current comprehensive clinicopathologic and imaging review. *Cancer Imaging* 2013;13:14-25
29. Madwed D, Mindelzun R, Jeffrey RB Jr. Mucocele of the appendix: imaging findings. *AJR Am J Roentgenol* 1992;159:69-72
30. Persaud T, Swan N, Torreggiani WC. Giant mucinous cystadenoma of the appendix. *Radiographics* 2007;27:553-557
31. Hale HL, Husband JE, Gossios K, Norman AR, Cunningham D. CT of calcified liver metastases in colorectal carcinoma. *Clin Radiol* 1998;53:735-741

32. Easson AM, Barron PT, Cripps C, Hill G, Guindi M, Michaud C. Calcification in colorectal hepatic metastases correlates with longer survival. *J Surg Oncol* 1996;63:221-225
33. Caseiro-Alves F, Brito J, Araujo AE, Belo-Soares P, Rodrigues H, Cipriano A, et al. Liver haemangioma: common and uncommon findings and how to improve the differential diagnosis. *Eur Radiol* 2007;17:1544-1554
34. Vilgrain V, Boulos L, Vullierme MP, Denys A, Terris B, Menu Y. Imaging of atypical hemangiomas of the liver with pathologic correlation. *Radiographics* 2000;20:379-397
35. Klotz T, Montoriol PF, Da Ines D, Petitcolin V, Joubert-Zakeyh J, Garcier JM. Hepatic haemangioma: common and uncommon imaging features. *Diagn Interv Imaging* 2013;94:849-859
36. Mitsudo K, Watanabe Y, Saga T, Dohke M, Sato N, Minami K, et al. Nonenhanced hepatic cavernous hemangioma with multiple calcifications: CT and pathologic correlation. *Abdom Imaging* 1995;20:459-461
37. Djouhri H, Arrivé L, Bouras T, Martin B, Monnier-Cholley L, Tubiana JM. Diffuse cavernous hemangioma of the rectosigmoid colon: imaging findings. *J Comput Assist Tomogr* 1998;22:851-855
38. Yoo S. GI-associated hemangiomas and vascular malformations. *Clin Colon Rectal Surg* 2011;24:193-200
39. Levy AD, Abbott RM, Rohrmann CA Jr, Frazier AA, Kende A. Gastrointestinal hemangiomas: imaging findings with pathologic correlation in pediatric and adult patients. *AJR Am J Roentgenol* 2001;177:1073-1081
40. Hsu RM, Horton KM, Fishman EK. Diffuse cavernous hemangiomatosis of the colon: findings on three-dimensional CT colonography. *AJR Am J Roentgenol* 2002;179:1042-1044
41. Outwater EK, Siegelman ES, Hunt JL. Ovarian teratomas: tumor types and imaging characteristics. *Radiographics* 2001;21:475-490
42. Park SB, Kim JK, Kim KR, Cho KS. Imaging findings of complications and unusual manifestations of ovarian teratomas. *Radiographics* 2008;28:969-983
43. Jung SE, Lee JM, Rha SE, Byun JY, Jung JI, Hahn ST. CT and MR imaging of ovarian tumors with emphasis on differential diagnosis. *Radiographics* 2002;22:1305-1325
44. Guinet C, Ghossain MA, Buy JN, Malbec L, Hugol D, Truc JB, et al. Mature cystic teratomas of the ovary: CT and MR findings. *Eur J Radiol* 1995;20:137-143
45. Buy JN, Ghossain MA, Moss AA, Bazot M, Doucet M, Hugol D, et al. Cystic teratoma of the ovary: CT detection. *Radiology* 1989;171:697-701
46. Friedman AC, Pyatt RS, Hartman DS, Downey EF Jr, Olson WB. CT of benign cystic teratomas. *AJR Am J Roentgenol* 1982;138:659-665
47. Saba L, Guerriero S, Sulcis R, Virgilio B, Melis G, Mallarini G. Mature and immature ovarian teratomas: CT, US and MR imaging characteristics. *Eur J Radiol* 2009;72:454-463
48. Moon W, Kim Y, Rhim H, Koh B, Cho O. Coexistent cystic teratoma of the omentum and ovary: report of two cases. *Abdom Imaging* 1997;22:516-518
49. Levy AD, Remotti HE, Thompson WM, Sobin LH, Miettinen M. Gastrointestinal stromal tumors: radiologic features with pathologic correlation. *Radiographics* 2003;23:283-304, 456; quiz 532
50. Miettinen M, Lasota J. Gastrointestinal stromal tumors: pathology and prognosis at different sites. *Semin Diagn Pathol* 2006;23:70-83
51. Ghanem N, Altehoefer C, Furtwängler A, Winterer J, Schäfer O, Springer O, et al. Computed tomography in gastrointestinal stromal tumors. *Eur Radiol* 2003;13:1669-1678
52. Tateishi U, Hasegawa T, Satake M, Moriyama N. Gastrointestinal stromal tumor. Correlation of computed tomography findings with tumor grade and mortality. *J Comput Assist Tomogr* 2003;27:792-798
53. Kim HC, Lee JM, Choi SH, Kim KW, Kim SH, Lee JY, et al. Imaging of gastrointestinal stromal tumors. *J Comput Assist Tomogr* 2004;28:596-604
54. Law JK, Ahmed A, Singh VK, Akshintala VS, Olson MT, Raman SP, et al. A systematic review of solid-pseudopapillary neoplasms: are these rare lesions? *Pancreas* 2014;43:331-337
55. Choi JY, Kim MJ, Kim JH, Kim SH, Lim JS, Oh YT, et al. Solid pseudopapillary tumor of the pancreas: typical and atypical manifestations. *AJR Am J Roentgenol* 2006;187:W178-W186
56. Buetow PC, Buck JL, Pantongrag-Brown L, Beck KG, Ros PR, Adair CF. Solid and papillary epithelial neoplasm of the pancreas: imaging-pathologic correlation on 56 cases. *Radiology* 1996;199:707-711
57. Ramage JK, Ahmed A, Ardill J, Bax N, Breen DJ, Caplin ME, et al. Guidelines for the management of gastroenteropancreatic neuroendocrine (including carcinoid) tumours (NETs). *Gut* 2012;61:6-32
58. Sahani DV, Bonaffini PA, Fernández-Del Castillo C, Blake MA. Gastroenteropancreatic neuroendocrine tumors: role of imaging in diagnosis and management. *Radiology* 2013;266:38-61
59. Heller MT, Shah AB. Imaging of neuroendocrine tumors. *Radiol Clin North Am* 2011;49:529-548, vii
60. Lewis RB, Lattin GE Jr, Paal E. Pancreatic endocrine tumors: radiologic-clinicopathologic correlation. *Radiographics* 2010;30:1445-1464
61. Buetow PC, Parrino TV, Buck JL, Pantongrag-Brown L, Ros PR, Dachman AH, et al. Islet cell tumors of the pancreas: pathologic-imaging correlation among size, necrosis and cysts, calcification, malignant behavior, and functional status. *AJR Am J Roentgenol* 1995;165:1175-1179
62. Poultsides GA, Huang LC, Chen Y, Visser BC, Pai RK, Jeffrey RB, et al. Pancreatic neuroendocrine tumors: radiographic calcifications correlate with grade and metastasis. *Ann Surg Oncol* 2012;19:2295-2303
63. Kim DW, Kim HJ, Kim KW, Byun JH, Song KB, Kim JH, et al. Neuroendocrine neoplasms of the pancreas at dynamic enhanced CT: comparison between grade 3 neuroendocrine carcinoma and grade 1/2 neuroendocrine tumour. *Eur Radiol* 2015;25:1375-1383
64. Low G, Panu A, Millo N, Leen E. Multimodality imaging of neoplastic and nonneoplastic solid lesions of the pancreas.

Radiographics 2011;31:993-1015
65. Rha SE, Byun JY, Jung SE, Chun HJ, Lee HG, Lee JM. Neurogenic tumors in the abdomen: tumor types and imaging characteristics. *Radiographics* 2003;23:29-43
66. Kim TJ, Han JK, Kim YH, Kim TK, Choi BI. Castleman disease of the abdomen: imaging spectrum and clinicopathologic correlations. *J Comput Assist Tomogr* 2001;25:207-214
67. Ko SF, Hsieh MJ, Ng SH, Lin JW, Wan YL, Lee TY, et al. Imaging spectrum of Castleman's disease. *AJR Am J Roentgenol* 2004;182:769-775
68. Bonekamp D, Horton KM, Hruban RH, Fishman EK. Castleman disease: the great mimic. *Radiographics* 2011;31:1793-1807
69. Meador TL, McLarney JK. CT features of Castleman disease of the abdomen and pelvis. *AJR Am J Roentgenol* 2000;175:115-118
70. Hill AJ, Tirumani SH, Rosenthal MH, Shinagare AB, Carrasco RD, Munshi NC, et al. Multimodality imaging and clinical features in Castleman disease: single institute experience in 30 patients. *Br J Radiol* 2015;88:20140670